Fresh and hardened properties of self-compacting concrete containing recycled fine clay brick aggregates

Zhang, Hongzhi; Yuan, Huaqiang ; Ge, Zhi; Wu, Jiajie ; Fang, Cheng; Schlangen, Erik; Šavija, Branko

DOI
10.1617/s11527-021-01751-5

Publication date
2021

Document Version
Final published version

Published in
Materials and Structures

Materials and Structures (2021)54:159
https://doi.org/10.1617/s11527-021-01751-5

ORIGINAL ARTICLE

Fresh and hardened properties of self-compacting concrete containing recycled fine clay brick aggregates

Hongzhi Zhang · Huaqiang Yuan · Zhi Ge · Jiajie Wu · Chen Fang · Erik Schlangen · Branko Šavija

Received: 12 January 2021 / Accepted: 2 July 2021

Abstract Clay brick is one of the major components of demolition waste, which is generally landfilled. Effective and new uses of recycled clay brick may provide sustainability benefits in terms of landfill reduction. Therefore, this research aims at applying Recycled fine clay brick aggregates (RFCBA) with sizes from 0.075 mm–4.75 mm to prepare Self-compacting concrete (SCC). The effects of RFCBA on fresh and hardened properties of SCC were investigated. Saturated surface dry RFCBA was used to replace Natural fine aggregate (NFA) with the percentage of 25%, 50%, 75% and 100%, respectively, in making the SCC mixes. Although experimental results showed that the flowability, passing ability, and segregation resistance of SCC containing RFCBA (RFCBA-SCC) decreased with the increasing RFCBA content, these properties still satisfy the criteria of SCC. The compressive strength, splitting strength, flexural strength, and elastic modulus of the RFCBA-SCC mixes decreased with an increase of RFCBA content. Due to their porous nature, recycled fine clay brick aggregates may also be a source of additional water for internal curing. The internal curing effect was confirmed by the mercury intrusion porosimetry, X-ray diffraction, and thermogravimetric analysis measurements. Moreover, a significant autogenous shrinkage reduction of SCC is achieved by using the RFCBA due to the release of additional water pre-stored in the RFCBA. Therefore, it can be concluded that the addition of RFCBA to SCC mixtures can provide additional practical benefits in the hardened state.

Keywords Recycled fine clay brick aggregate · Self-compacting concrete · Rheology properties · Mechanical properties · Microstructures

Supplementary Information The online version contains supplementary material available at https://doi.org/10.1617/s11527-021-01751-5.

H. Zhang · H. Yuan · Z. Ge (✉) · J. Wu · C. Fang
School of Qilu Transportation, Shandong University, 250002 Jinan, People's Republic of China
e-mail: zhige@sdu.edu.cn

H. Zhang
Suzhou Research Institute, Shandong University, Suzhou 215021, People's Republic of China

E. Schlangen · B. Šavija
Faculty of Civil Engineering and Geosciences, Microlab, Delft University of Technology, Stevinweg 1, 2628 CN Delft, The Netherlands

Published online: 13 July 2021

1 Introduction

Due to its unique characteristics, e.g., high flowability, passing ability, and resistance to segregation, the use of Self-compacting concrete (SCC) has gained wide acceptance in recent years. As no vibration is required, it significantly reduces the noise on the construction

site and the labour needed for concrete placement. Moreover, as it can flow under its own weight and maintain sufficient resistance to segregation, SCC has excellent applicability for elements with complicated shapes and congested reinforcement.

Generally, a high binder content is usually used to achieve a good segregation resistance [1]. Supplementary cementitious materials are generally added to improve the flowability and to reduce the amount of superplasticizer [2–4]. As SCC possess a high cement content, the autogenous shrinkage becomes significant [5], because of the greater volume of small-diameter pores and the available water reduction [6]. This leads to potential early-age cracking, which is a big concern for service life. Furthermore, conventional curing does little to mitigate the autogenous shrinkage of SCC, as the water from the external surface only affects the concrete to a limited depth [7]. An effective way of mitigating autogenous shrinkage is to use internal curing. Two common approaches can be applied: the addition of Superabsorbent polymers (SAP) or Lightweight aggregates (LWA). The first method entails adding SAPs into the concrete mixture. During mixing, the SAP absorbs water and swells [8]. Water stored in the SAP is released when self-desiccation happens. The study carried out by Jensen and Hansen [9] showed that with 0.6% addition of SAP, self-desiccation in cement paste having w/c of 0.3 could be completely avoided. The second way is to use the pre-saturated porous LWA. During cement hydration, LWA releases water to the surrounding paste to replace moisture lost and reduce self-desiccation [10].

It is found that the recycled aggregate has a high water absorption capacity. Therefore, there exists a potential to use it for internal curing [11]. With respect to the recycled concrete aggregate, a water absorption capacity larger than 10% is found because of the adherent cement mortar. In contrast, the natural aggregates possess a water absorption capacity, in general, less than 1% [12–14]. Yildirim et al. [15] reported that the drying shrinkage can be satisfactorily reduced with a recycled concrete aggregate content of 50%. However, because of the limited porosity and water absorption ability, it has a limited effect on the autogenous shrinkage of low w/c ratio mortar [11]. Clay brick belongs to another type of recycled aggregate. Compared to crushed concrete aggregate, recycled clay brick has a much higher porosity (around 20% [16–20]) and water absorption (between 15–28% [21–24]). However, its high water absorption is generally considered to harm the mechanical properties of concrete. Reference [25] reports that using recycled clay brick as a replacement for coarse aggregate leads to a reduction in both compressive and tensile strengths. Extensive studies [26, 27] show that it is possible to make concrete having strength in between 20 and 30 MPa can be made using the recycled clay brick within a replacement no more than 50%. Consequently, the application of recycled clay brick in construction is limited. Therefore, in order to exploit vast amounts of recycled clay brick aggregates that are available, its utilization in SCC is desirable [28].

To reduce the autogenous shrinkage of SCC, this work proposes to use Recycled fine clay brick aggregates (RFCBA) possessing a size range from 0.075–4.75 mm to replace natural fine aggregate. The replacement level was chosen as 25%, 50%, 75% and 100%, respectively. First, the fresh properties of the prepared SCC containing RFCBA (RFCBA-SCC) were examed to ensure the prepared mixes meet the flowing and passing ability requirement of SCC. The influence of the RFCBA content on the microstructure, mechanical properties, and autogenous shrinkage were studied. It is expected that this study would provide a more promising way for reuse of clay brick.

2 Materials and methods

2.1 Materials

Ordinary Portland cement 42.5 I purchased from China United Cement Corporation and Class F fly ash were used as the binder. Their chemical compositions and physical properties are presented in Table S1 and S2, respectively. The gradation of used fine and coarse aggregates are shown in Figure S1. With regard to the fine aggregate, local natural river sand and waste clay brick obtained from a demolition site were used. The X-ray diffraction (XRD) measurement presented in Figure S2 shows that quartz, hematite, and rutile are the main mineral compositions in clay brick. The brick was first broken up and sieved to different sizes. To produce the recycled fine clay brick aggregate (RFCBA) with designed gradation, the sieved bricks were recombined. Table S3 presents the physical properties of natural fine aggregate (NFA) together

with RFCBA. Mercury intrusion porosimetry was used to measure the porosity, and water absorption was measured according to ASTM C1761/C1761M—17 [29]. Although two types of aggregate have the same grading, the RFCBA has a smaller apparent density and greater water absorption ability because of its porous microstructure. Figure S3 presents the pore size distribution of the RFCBA and NFA. More than 95% percolated pore (28.33% by volume) is greater than 100 nm showing that the RFCBA can be efficiently used for internal curing, as it has been proved the pore with size larger than 100 nm [30–32] can supply water effectively during self-desiccation. The absorption and desorption ability of the RFCBA have been reported in the authors' previous work [33]. The absorption measurements show that the RFCBA could be saturated in a relatively short period with an absorption larger than 10 wt.%, which is much larger than the criteria (5 wt.% for 72 h absorption) specified by ASTM C 1761/1761 M - 17 [29]. While the desorption measurements indicate that the desorption speed increases with the reduction of the RH ambient. With respect to 59% RH ambient, most of the absorbed water releases within 10 days. In terms of 97% RH ambient, less than 20% absorbed water has been disported after 10 days. This indicates that in the RFCBA-SCC, more water would come out at the late stage when the RH decreases due to the self-desiccation. In the current study, data from the desorption measurement is used to plot the isothermal desorption curve, see Fig. 1. It can be seen that the particle size has little influence on the isothermal desorption curve and more than 90% absorbed water is released at 59% RH ambient. In terms of coarse aggregate, crushed limestone having a water absorption of 0.58% was used. The workability was adjusted by the superplasticizer.

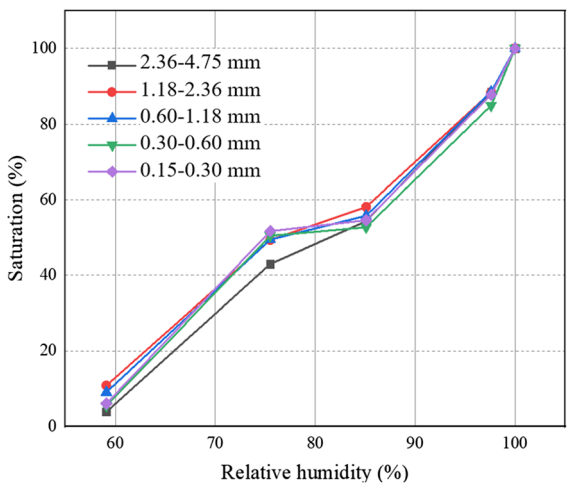

Fig. 1 Isothermal desorption curve of used RFCBA with different sizes

2.2 Mixture proportions

Five SCC mixes (including a reference mix) were designed and produced. Portland cement was blended with fly ash as a binder with a mass ratio of 3:2. Based on the Guidelines for SCC [34], the water to binder and binder to fine aggregate mass ratios were determined as 0.28 and 0.34 for all mixes. RFCBA in Saturated surface dry (SSD) condition was used as an internal curing agent to replace NFA. To reveal the effect of replacement level on SCC, NFA was replaced by the RFCBA with a percentage of 0%, 25%, 50%, and 75% 100% by volume, respectively, the amount of superplasticizer was 0.8% of binder weight. Table 1 shows the detailed mix proportions.

2.3 Testing method

2.3.1 Fresh properties measurements

The slump flow and L-box (with 2 rebars) tests were conducted according to BS EN 206–9 [35] and Guidelines for SCC [34]. The slump test characterizes the flowability and filling ability of the fresh SCC by measuring the mean diameter of the spread of fresh concrete using a conventional slump cone. T_{500} can be used to estimate the viscosity of SCC. It records the flow time for the fresh mixture getting to 500 mm after lifting a cone. With respect to the L-box test, a passing ratio is used to indicate the passing ability of the SCC mix.

2.3.2 Microstructural characterization

To characterize the internal curing effect of the SSD RFCBA, mortar specimens were prepared with the 4.75 mm grade aggregates and blends of cement and fly ash (mass ratio 3:2). A w/b ratio of 0.28 was used. The mixing procedure was conducted following the EN 196–3:2005 + A1:2008 (E) standard [36]. Cylindrical plastic moulds with a size of 30 mm in mm diameter and 60 mm in height were used for casting.

Table 1 Mix proportions of SCC (kg/m^3)

Mix	NFA replacement level (%)	Water (kg/m^3)	Cement (kg/m^3)	Fly ash (kg/m^3)	Coarse aggregate (kg/m^3)	NFA (kg/m^3)	RFCBA (kg/m^3)	Superplasticizer (kg/m^3)
Ref	0	149.5	321	214	854	806	0	4.28
R25	25	149.5	321	214	854	605	160	4.28
R50	50	149.5	321	214	854	403	321	4.28
R75	75	149.5	321	214	854	202	482	4.28
R100	100	149.5	321	214	854	0	642	4.28

10 SSD RFCBAs (4.75 mm) were added into the fresh mixture in one cylinder, while in the other one, the same amount and sized NFA was used. Afterward, the cylinders were sealed and stored in lab conditions (temperature: 20 ± 1 °C). After 28 days of curing, mortars were cut. Pastes within 2 mm distance to the aggregates were taken for the Mercury Intrusion Porosimetry, thermogravimetric/derivative thermogravimetric analysis (TG/DTG) and XRD tests. The solvent exchange approach [37] was adopted to arrest the hydration. In this approach, isopropanol was used. The specimens were dried in the vacuum champer under a pressure of 0.5 MPa and a temperature of 45 °C for drying until no weight change can be monitored.

Porosity and pore size distribution were measured at 28 days using MIP on the dried cement paste [38]. An Autopore II 9220 device was used. The relation between pressure p(MPa) and the pore diameter d(μm) is described by the Washburn equation [39] based on a model of cylindrical pores:

$$p = -\frac{4\gamma \cos\theta}{d} \quad (1)$$

where θ is the contact angle between the mercury and the surface of cement, and γ the surface tension of mercury. For the measurement, the contact angle and the surface tension were set to 139° and 485 mN/m, respectively. The pressure capacity of the mercury intrusion porosimeter is 4.00×10^{-3}–4.13×10^{2} MPa, leading to the measured pore size within the range of 7 nm–314 μm.

To investigate the internal curing effect, both TG/DTG and X-XRD were conducted on hardened cement paste. The pastes were grounded to a powder for the following test.

TG/DTG test was performed by using TA Instruments SDT-Q600 to identify H_2O and $Ca(OH)_2$ emissions for each temperature range. The TG/DTG test was conducted using N_2 gas with a flow rate of 100 ml/min and a heating rate of 10 °C/min within a temperature interval between 100 °C and 1000 °C.

XRD tests were conducted using a Rigaku D/MAX-RA XRD diffractometer. During the test, the Cu-Kα radiation was set as 40 kV and 40 mA with a scanning speed of 0.02 °/s over the range of 5—90 °.

The interface between RFCBA and cement paste matrix was investigated with a SU-70 Scanning Electron Microscope (SEM). Crushed SCC specimens were then polished with sandpapers and diamond paste in which 1 μm diamond paste was used for the last polishing. Samples were then coated by evaporation with gold. Backscattered electrons (BSE) mode was used to scan the polished surfaces.

2.3.3 Strength and elastic properties measurements

Compressive, flexural, and tensile strengths and modulus of elasticity were measured following the Chinese GB/T 11,969–2008 standard [40]. For each mix, specimens with dimensions described in Table S4 were cast and used for the corresponding test. After casting, the specimens were cured for 24 h under sealed condition under a temperature of 20 ± 1 °C. Subsequently, the samples were demoulded and cured in a standard curing room with a temperature of 20 ± 1 °C and a relative humidity of 98% ± 2% until the test. Table S4 lists all the crucial parameters for the mechanical tests. For each condition, three specimens were measured.

2.3.4 Autogenous shrinkage and internal relative humidity measurements

Autogenous shrinkage is a dominant factor for cracking control for w/b ratio concrete, i.e., SCC [41]. Measurements of the internal relative humidity (RH) and autogenous shrinkage were performed to investigate the potential of RFCBA on the autogenous shrinkage mitigation and its mechanism behind.

For internal relative humidity (RH) measurements, cast-in sensors with acceptable accuracy of ± 0.1% were used. A PVA tube was positioned at the middle depth of the cubic specimen (100 mm). A glass bar was inserted into the PVA tube before casting to prevent concrete from flowing into the PVA tube. After casting the SCC into a paraffin wax made mould, a plastic sheet was used to cover the specimen surface. After one day curing, a Vaisala HMP42 humidity sensor was used to replace the glass bar. The hole was then sealed by using epoxy resin. Paraffin wax was used to seal the top surface of the specimen to avoid any moisture exchange between the specimen and the environment. It is worth mentioning that the sensor has been calibrated out before the RH measurements at a constant temperature of 20 °C. In the calibration procedure, distilled water and saturated salt solutions with known RH values of 11% (LiCl), 33% ($MgCl_2$), 43%(K_2CO_3), 59%(NaBr), 70%(KI), 75%(NaCl), 85%(KCl), 91% ($BaCl_2$) and 98% (K_2SO_4) were used. For each RH condition, the sensor was placed in a sealed container with the corresponding solution. After each measurement, the sensor was corrected if the measured value did not match the theoretical one.

With respect to autogenous shrinkage measurement, a stainless-steel mould consisting of two reflecting targets at the ends was used, see Figure S4. The two reflecting targets are free to move with the cast specimens. Eddy current sensors were used to measure movement of the reflecting targets continuously.The measuring accuracy of deformation is smaller than 2 μm. The autogenous strain was calculated as:

$$\varepsilon = \frac{d_1 + d_2}{L} \quad (2)$$

where d_1 and d_2 are the movement measured by the two sensors, L the initial length of the casted specimen. The length of the specimens was 515 mm, and the cross-section was 100 mm × 100 mm. After casting, the specimens were sealed by polystyrene sheets to avoid moisture loss. Measurements were started 1 h after the casting. For each mixture, 3 specimens were tested. Strain was recorded every hour consecutively for 7 days. The average value represented the shrinkage strain. The environmental temperature was kept at 20 ± 2 °C during the test.

3 Results and discussions

3.1 Fresh properties

Table 2 shows the measurements of slump flow, T_{500}, J-ring spread value as well as blocking ratio. It is evident that the increase in replacement ratio causes a reduction in the flowability. With 100% replacement, a reduction of 12% is observed for the slump flow, while 11.06% for the J-ring test. Consequently, it takes a longer period for the mixture to flow to 500 mm. Nevertheless, the slump flowability meets the criteria for SF2 (640–800 mm), which is suitable for many normal applications [34]. The difference between slump flow and J-ring spread diameter is smaller than 25 mm, which means its passing ablitiy belongs to the PA2 as specified by the Chinese technical specification (Technical Specification for Application of Self-compacting Concrete, JGJ/T283-2012) [42]. Furthermore, the blocking ratio decreases from 0.82 to 0.73, with replacement level of NFA increasing from 0 to 100%. This can be caused by stronger cohesion between cement paste and RFCBA, compared with NFA. This is in accordance with [43] but in contrast with [44]. However, in [44], additional water was added during mixing to prepare the SCC. According to [34], the prepared SCC containing 100% RFCBA maintains adequate passing ability (0.70).

3.2 MIP results

In Fig. 2, the capillary pore size distribution of cement paste mixes around different types of aggregate is shown. The critical pore diameter is assumed as the peak in the differential pore size distribution [38]. The critical pore diameter decreases when RFCBA is used. Figure 3 shows the relative frequency of the pore size distribution. The paste in the vicinity of RFCBA tends to have smaller pores. Specifically, most pores fall in the range between 20–50 nm for the NFA-mortar,

Table 2 Measured fresh properties of RA-SCC mixtures

Replacement level (%)	Slump flow (mm)	T_{500} (s)	J-ring spread diameter (mm)	Blocking ratio
0	745.2	3.75	719.0	0.82
25	707.0	4.53	678.5	0.80
50	696.3	6.43	669.0	0.79
75	663.8	7.68	654.3	0.75
100	652.8	8.59	636.5	0.73

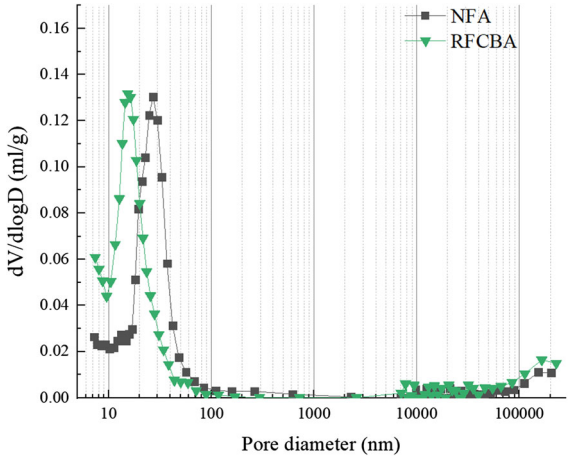

Fig. 2 Influence of RFCBA on the pore size distribution

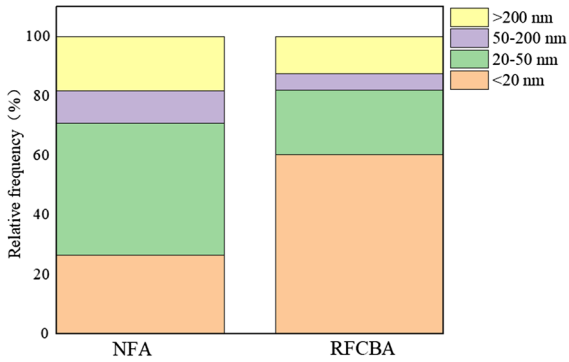

Fig. 3 Influence of RFCBA on the relative frequency of pore size distribution

while with the use of RFCBA, more than 50% of the pore volume has a size smaller than 20 nm. Table 3 shows the measured percolated pore volume. The use of RFCBA has a remarkable influence on the pore volume leading to a lower porosity, because the internal curing effect causes further hydration of cement paste, which reduces the porosity and pore size [45]. However, it is important to note that pores smaller than 6 nm (gel pores) are not accessible by the MIP test. To characterize the gel pore, helium pycnometry [46] or nitrogen adsorption test [47] is required.

3.3 TG/DTG and XRD results

The results of the TG/DTG are given in **Fig. 4**. Assuming that the vacuum drying removes all free water [48], the TG measurement can provide a measure of the amount of hydrate water. A peak at 100–125 °C is observed in DTG because of the dehydration of ettringite and C-S-H [49]. However, the amount of the two phases cannot be quantified because their peaks are overlapped. The dehydration of calcium hydroxide leads to a peak of DTG in the temperature interval around 450 °C. This peak can be used to calculate the amount of calcium hydroxide. In the temperature 600–800 °C, carbonate phases (i.e., $CaCO_3$) decompose, introducing a small peak in the DTG. As reported by Weerdt et al.[50], the amount of hydrate water (H) and calcium hydroxide (CH) are expressed as % of the dry sample weight at 550 °C (ω_{550}):

$$H = \frac{\omega_{100} - \omega_{500}}{\omega_{550}} \tag{3}$$

$$CH = \frac{\omega_{450} - \omega_{550}}{\omega_{550}} \cdot \frac{74}{18} \tag{4}$$

(*)Ca(OH)2 (74 g/mol) → CaO + H2O (18 g/mol) weight difference determined using stepwise method. Table 4 shows the calculated amount of hydrate water (H) and calcium hydroxide (CH). Clearly, at 28 days, the use of SSD RFCBA leads to an increase of bound water and calcium hydroxide in the surrounding cement paste. As reported by [51], when the content

Table 3 The effect of fine aggregate type on porosity, average pore size, and critical pore diameter

Aggregate type	Porosity (%)	Average pore diameter (nm)	Critical pore diameter (nm)
NFA	15.26	16.26	27.14
RFCBA	11.31	11.48	13.19

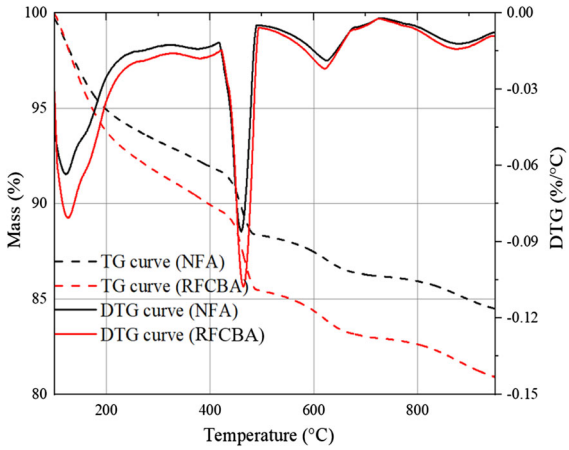

Fig. 4 Results of TG/DTG results

Table 4 Amount of calcium hydroxide and hydrate water content for SCC containing a different type of aggregates

Aggregate type	CH (wt.%)	H (wt.%)
NFA	13.66	11.57
RFCBA	16.11	14.52

of fly ash is larger than 30% (40% in the current study), the absorption of fly ash is over the released energy of cement after 7 days. Since calcium hydroxide is mainly produced by the hydration of cement, the TG/DTG measurements tend to confirm that a higher degree of hydration is achieved through using the SSD RFCBA.

Figure 5 shows the recorded XRD diffractograms along with identified mineral phases for pastes taken from different mixes. All pastes show peaks for calcium hydroxide, alite, belite, ettringite, and C_4AF, which are the dominating minerals presented in hydrated Portland cement paste. No other peak corresponding to the other mineral phase is observed. Moreover, when RFCBA is used, the intensity calcium hydroxide increases and intensities of alite and belite

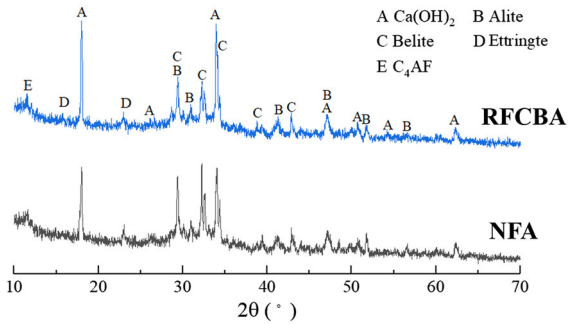

Fig. 5 Influence of fine aggregate type on mineral phases presented in the hardened cement paste matrix

decrease, proving the internal curing effect of RFCBA as discussed above.

Figure 6 shows the interface between RFCBA and cementitious paste. Unlike the NFA [52], no clear bond is found between RFCBA and paste. Due to the internal curing effect, few anhydrous cement grains remain close to the RFCBA, indicating a much higher hydration degree has been reached by using the pre-wetted RFCBA. Furthermore, a large number of big open pores exist in the RFCBA. These pores allow the entrance of cement particles during the mixing and provide sites for the hydrated cement paste to merge across the interface, improving the interaction between RFCBA and the cement matrix [53]. It is similar to lightweight aggregate concrete. Therefore, cracks do not follow the interface, but often also pass through aggregates [54].

3.4 Strengths and elastic moduli

Figure 7 presents the effect of replacement level on the strengths and elastic modulus of the RFCBA-SCC specimens. Figure 7a presents the development of compressive strength. After 3 days, there is a marked difference among RFCBA-SCCs incorporating different amounts of RFCBA: the increasing of fine aggregate replacement level reduces the compressive strength. With a 25% replacement of RFCBA, a slight

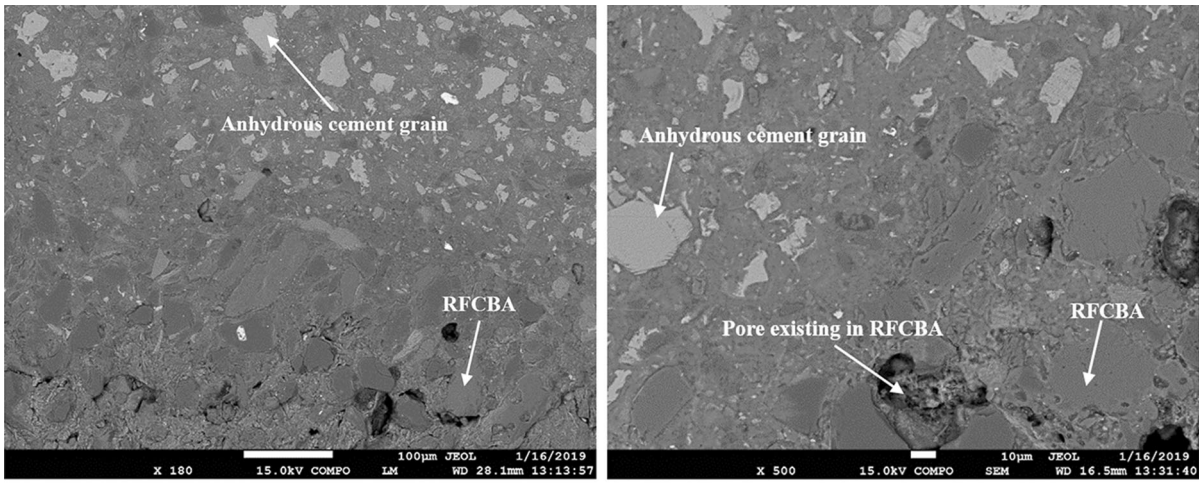

(a) (b)

Fig. 6 BSE micrographs of the interface between RFCBA and hardened cement paste: (**a**) low magnification (× 180); (**b**) high magnification (× 500)

increase is observed for the 3-d compressive strength. In general, no significant compressive strength reduction is observed for the replacement level of 25%, while a reduction of around 20% is found for the replacement level of 100%. Flexural strength is shown in Fig. 7b, while splitting strengths are presented in Fig. 7c. The same trends are observed. The tensile strengths decrease less than the compressive strength [55–57]. This can be attributed to the fact that in regular concrete, tensile failure is mainly governed by the weakest ITZ [58]. With respect to the RFCBA-SCC, a well-bonded interface is formed, which results in higher tensile strength. The 28-d elastic modulus shown in Fig. 7d is in accordance with the strength development, especially the 28-d compressive strength.

Figure 8 presents the relationship between the measured tensile and compressive strengths. A determination coefficient (R^2) greater than 0.98 observed. This indicates that tensile strength and compressive strength are linearly dependent in RFCBA-SCC. Furthermore, as expected, flexural strength is higher than splitting strength because larger pure tension volume exists in the latter [55]. In Fig. 8b, a linear equation is adopted to exploit the compressive strength-elastic modulus relationship with a determination coefficient of 0.94. These observations are in accordance with other studies [59–62]. It is worth to mention that the fitted linear relationships are only suitable for the limited compressive range (35–65 MPa) in the current study. In terms of a wider range compressive strength, the linear relationships do not apply. In return, the tensile-compressive strength and elastic modulus-compressive strength ratios decrease with the increasing of the compressive strength [63].

3.5 Internal curing effect

Figure 9 show the measured autogenous shrinkage of RA-SCC with various NFA replacement level. As expected, the shrinkage strain increases rapidly in the first few days. Because of the low w/b ratio, the reference SCC made with NFA has high shrinkage, i.e., 800×10^{-6} at 7 days. The shrinkage is significantly reduced by using the pre-wetted RFCBA. At the replacement level of 50%, the deformation is reduced by about 50% of the reference. When the replacement level reaches 100%, the autogenous shrinkage is reduced to less than 100×10^{-6}. This can be attributed to the delayed drop of internal RH as discussed followings.

In Fig. 10, the evolution of internal RH between 1–7 days for RA-SCC specimens with the various percentage of RFCBA is given. In general, the RH decreases with elapsed time, and the rate is rather high in the first few days and then slows down gradually. Clearly, with the percentage of RFCBA increasing, the

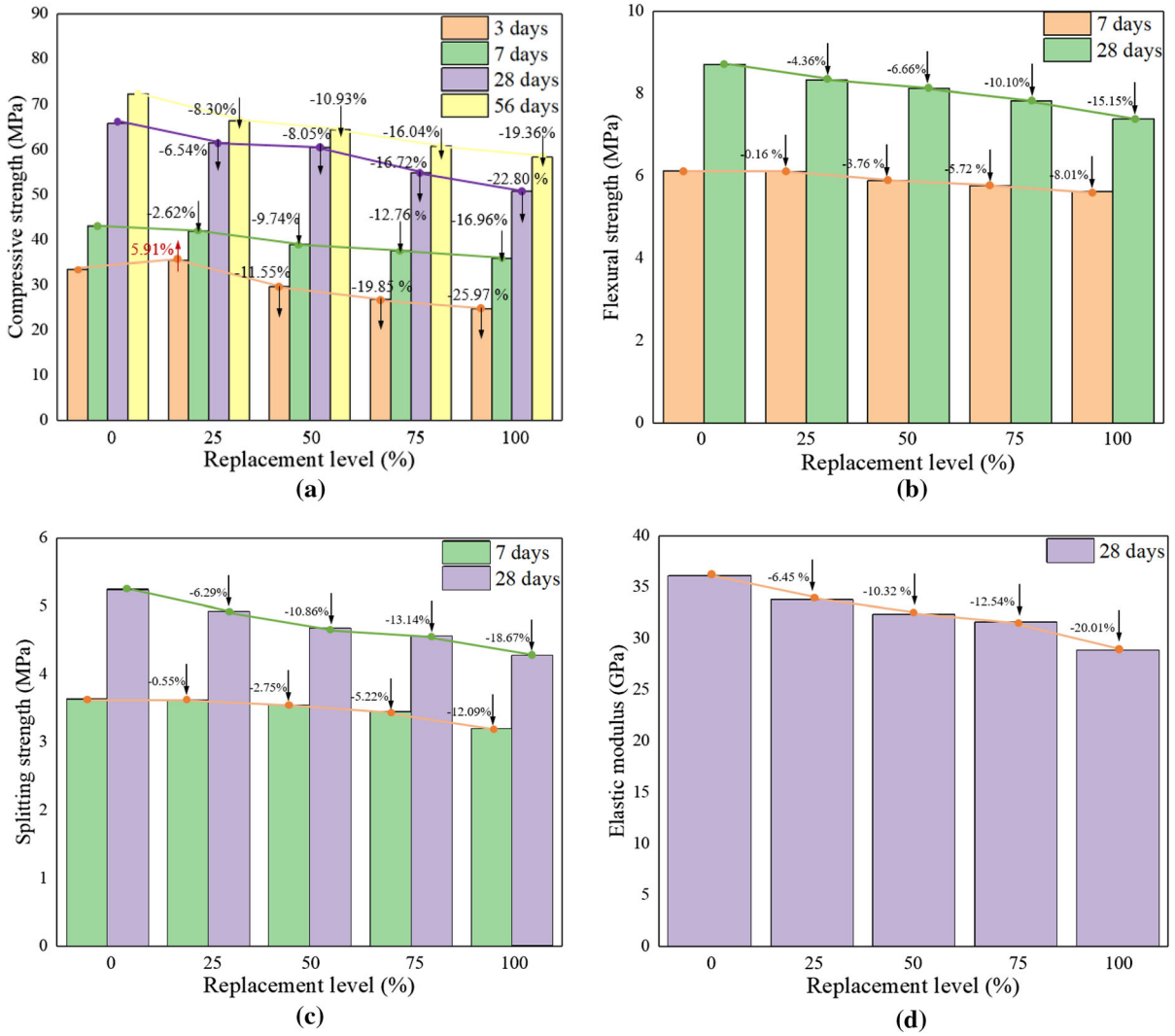

Fig. 7 Effect of fine aggregate replacement level on: (**a**) compressive strength; (**b**) flexural strength; (**c**) splitting strength; (**d**) elastic modulus

reduction of RH decreases. More promisingly, the reduction of RH on the first day has been significantly reduced by replacing the NFA with saturated RFCBA. These findings are consistent with autogenous shrinkage observations.

As a similar evolution trend is found between internal RH and autogenous deformation, **Fig. 11** plots the autogenous shrinkage and internal RH reduction (1-RH) together. Clearly, a linear relation can be found between the measured shrinkage strain and RH reduction. Similar trends are observed in cement paste [64], normal concrete [65] and lightweight concrete [66]. Thus, a linear regression equation was used to approximate the relationship between shrinkage deformation and the RH reduction [64]:

$$\varepsilon = -[a \cdot (1 - RH) + b] \times 10^{-6} \quad (5)$$

where ε is the autogenous shrinkage strain, a and b empirical fitting constants. A least-squares method was used for the regression. As shown in Fig. 11, the high value of the determination coefficient ($R^2 > 0.95$) confirms the shrinkage strain is strongly related to the RH reduction. However, it should be noticed that the slope of each mix is different. Higher RFCBA content results in a gentler slope. As found by

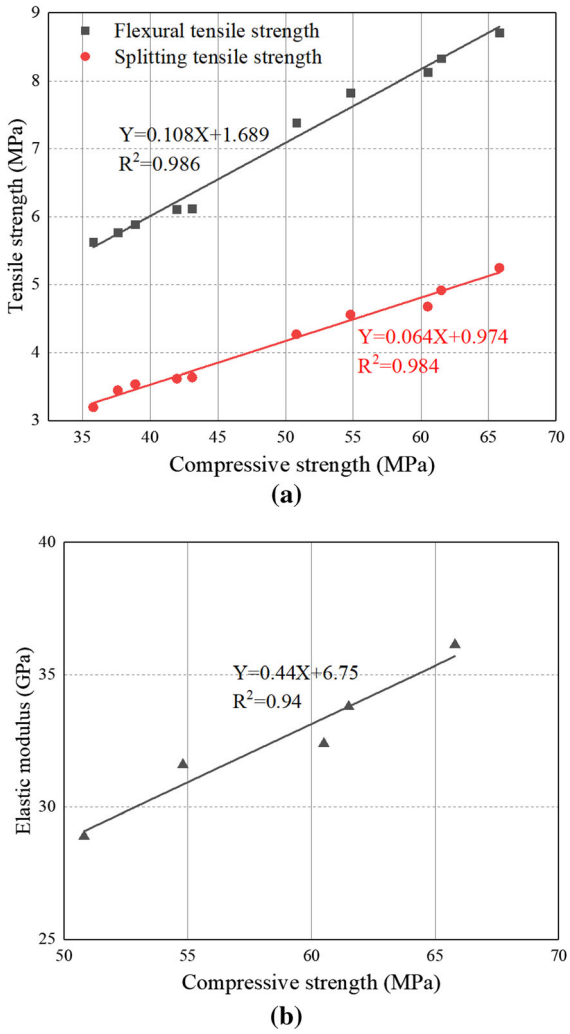

Fig. 8 Relationship between the compressive strength and (**a**) tensile strengths, (**b**) elastic modulus

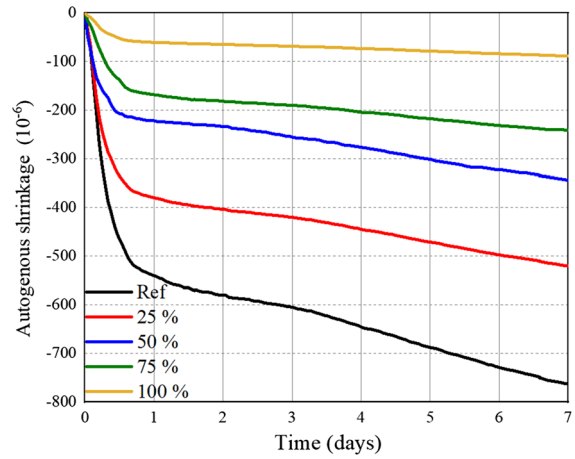

Fig. 9 Influence of fine aggregate replacement level on measured autogenous shrinkage

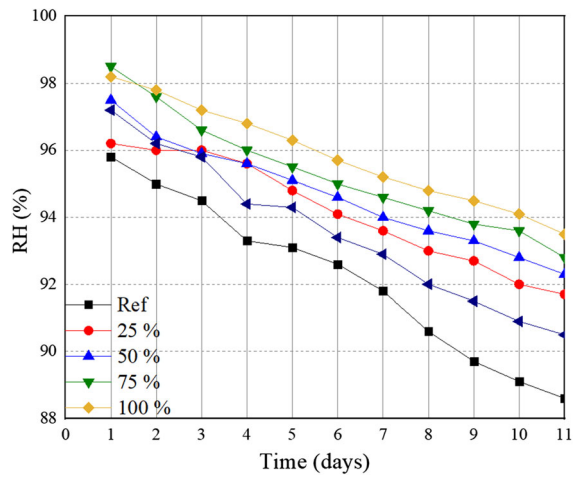

Fig. 10 Influence of fine aggregate replacement level on internal RH

Wei.et al. [64], regardless of the w/b ratio, the slope should be constant for cementitious paste. Thus, this difference can be introduced by the aggregate restraining effects [67]:

$$\varepsilon = \varepsilon_p \cdot (1 - V_A)^n \quad (6)$$

where ε_P is the shrinkage of net cement paste, V_A the aggregate volume fraction, n the parameter representing aggregate restraining effect. The gentle slope of the high RFCBA content mix indicates that the RFCBA has a higher aggregate restraining effect compared with the NFA, although it possesses lower elastic modulus. This can be possibly attributed to the following reasons: 1) The internal curing effect leads to a stronger matrix around the RFCBA, which enlarges the effectively restrained area; 2) Together with the internal curing effect, the rough and porous surface of RFCBA leads to the well-bounded interface between cement paste matrix and RFCBA. This enhances the restraining ability of RFCBA.

In the first 24 h, the microstructure of cement paste changes significantly with time. More complex mechanism including chemical shrinkage, creep and temperature change et.al should be considered for the deformation changes [7, 68]. Therefore, the linear relartionship relationship between RH drop and measured shrinkage is not validated. The fitted parameter

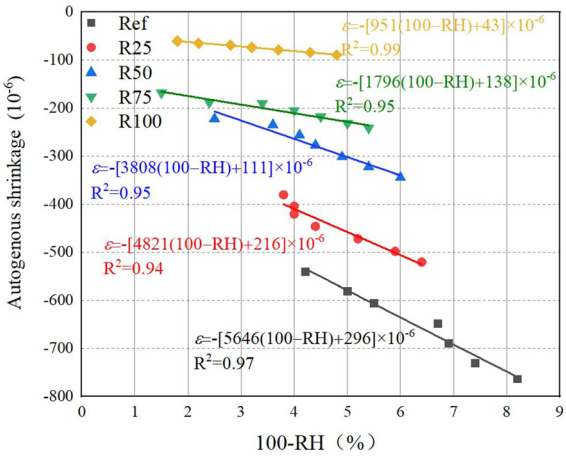

Fig. 11 Development of shrinkage along with internal RH drops

b may be used to represent the total deformation apart from the self-desiccation.

4 Conclusions

In this paper, SSD RFCBA was used to replace NFA for the purpose of internal curing for the SCC. Five mixes with different RFCBA content were investigated. Microstructural characterisation and meso-scale mechanical measures were carried out for a comprehensive understanding on the influence of RFCBA on the SCC performance. With the results presented in this study, the following conclusions can be drawn:

- Replacement of NFA with RFCBA decreases the flowability, passing ability and segregation resistance. However, even with the 100% replacement, it satisfies the criteria for SF2 (suitable for many normal applications) and maintains adequate passing ability.
- The MIP, TGA and XRD show the internal curing has been achieved by using the pre-saturated RFCBA. The BSE images show that a well-bounded ITZ exists between the RFCBA and cement paste.
- In general, with the increasing of RFCBA content, mechanical properties of the SCC decrease. With a replacement level of 25%, no significant drop in mechanical properties is observed, while for a replacement level of 100%, a reduction of around 20% for compressive strength and elastic modulus is found. Because of the well-bonded interface, the tensile strengths decrease less than compressive strength. Similar to normal concrete, a linear relationship between strengths and elastic modulus was found.
- Pre-wetted RFCBA can effectively delay the drop of internal RH in SCC attributed to the self-desiccation. The overall autogenous shrinkage of the RFCBA-SCC is therefore significantly reduced.
- The autogenous shrinkage possesses a linear relationship with the RH drop after 1 day curing and the solpe decreases with the increment of RFCBA content. This indicates that the SSD has a stronger restraining effect compared with NFA.

The using of RFCBA in SCC is promising as it can significantly reduce the autogenous shrinkage in the SCC, which offers a sustainable and economical solution in reusing of waste clay brick. Nevertheless, prior to the practical application, more comprehensive studies on the drying shrinkage and long-term performance are still required.

Funding This study was funded by National Natural Science Foundation of China (51478252, 51978387, 52008234), the Natural Science Foundation of Shandong Province (ZR2013EEM025), the Natural Science Foundation of Jiangsu Province (BK20200235), the Key Research and Development Program of Shandong Province (2015GSF122009) and Taishan Scholar Foundation of Shandong Province (tsqn201909032). Sincere gratitude is given to the research laboratory in the School of Qilu Transportation, Shandong University.

Declarations

Conflict of interest The authors declare that they have no conflict of interest.

References

1. Khayat KH (1999) Workability, testing, and performance of self-consolidating concrete. Mater J 96(3):346–353
2. Poon C, Ho D (2004) A feasibility study on the utilization of r-FA in SCC. Cem Concr Res 34(12):2337–2339
3. Kurita M, Nomura T (1998) Highly-flowable steel fiber-reinforced concrete containing fly ash. Spec Publ 178:159–176
4. Kou SC, Poon CS (2009) Properties of self-compacting concrete prepared with recycled glass aggregate. Cem Concr Compos 31(2):107–113

5. Aitcin P-C (1999) Demystifying autogenous shrinkage. Concr Int 21(11):54–56
6. Zhang M, Tam C, Leow M (2003) Effect of water-to-cementitious materials ratio and silica fume on the autogenous shrinkage of concrete. Cem Concr Res 33(10):1687–1694
7. Lura P (2003) Autogenous deformation and internal curing of concrete. Delft University, Delft, The Netherlands
8. Jensen OM, Hansen PF (2001) Water-entrained cement-based materials: I Principles and theoretical background. , Cem Concr Res 31(4):647–654
9. Jensen OM, Hansen PF (2002) Water-entrained cement-based materials: II Experimental observations . Cem Concr Res 32(6):973–978
10. Mehta P (1992) Materials Science of Concrete II. Cem Concr Aggreg 14(1):69–69
11. H. Kim, D. Bentz, Internal curing with crushed returned concrete aggregates for high performance concrete
12. Gómez-Soberón JM (2002) Porosity of recycled concrete with substitution of recycled concrete aggregate: An experimental study. Cem Concr Res 32(8):1301–1311
13. Katz A (2003) Properties of concrete made with recycled aggregate from partially hydrated old concrete. Cem Concr Res 33(5):703–711
14. Pepe M, Toledo Filho RD, Koenders EA, Martinelli E (2014) Alternative processing procedures for recycled aggregates in structural concrete, Constr Build Mater. 69(1): 124–132
15. Yildirim ST, Meyer C, Herfellner S (2015) Effects of internal curing on the strength, drying shrinkage and freeze–thaw resistance of concrete containing recycled concrete aggregates. Constr Build Mater 91:288–296
16. Otoko R (2014) Use of crushed clay bricks as aggregate in concrete. Int J Eng Technol Res 2:1–9
17. Angulo SC, Carrijo PM, Figueiredo AD, Chaves AP, John VM (2009) On the classification of mixed construction and demolition waste aggregate by porosity and its impact on the mechanical performance of concrete. Mater Struct 43(4):519–528
18. Zong L, Fei Z, Zhang S (2014) Permeability of recycled aggregate concrete containing fly ash and clay brick waste. J Clean Prod 70:175–182
19. Ge Z, Gao Z, Sun R, Zheng L (2012) Mix design of concrete with recycled clay-brick-powder using the orthogonal design method. Constr Build Mater 31:289–293
20. Ge Z, Wang Y, Sun R, Wu X, Guan Y (2015) Influence of ground waste clay brick on properties of fresh and hardened concrete. Constr Build Mater 98:128–136
21. Bolouri Bazaz J, Khayati M (2012) Properties and performance of concrete made with recycled low-quality crushed brick. J Mater Civ Eng 24(4):330–338
22. Zhang S, Zong L (2014) Properties of concrete made with recycled coarse aggregate from waste brick. Environ Prog Sustain Energy 33(4):1283–1289
23. Aliabdo AA, Abd-Elmoaty A-EM, Hassan HH (2014) Utilization of crushed clay brick in concrete industry. Alex Eng J 53(1):151–168
24. Ge Z, Yue H, Sun R (2015) Properties of mortar produced with recycled clay brick aggregate and PET. Constr Build Mater 93:851–856
25. Afify MR, Soliman NM (2014) Improvement properties of recycle concrete using clay brick as a coarse aggregate. Int J Curr Eng Technol 4(1):119–127
26. Mohammed TU, Hasnat A, Awal MA, Bosunia SZ (2014) Recycling of brick aggregate concrete as coarse aggregate. J Mater Civ Eng 27(7):B4014005
27. Liu Q, Zhang XN (2014) Expermental study on the mixture ratio and the compressive strength of concrete with Recycle crushed brick coarse Aggregate. Trans Tech Publ, Applied Mechanics and Materials, pp 1362–1365
28. Hu J, Wang Z, Kim Y (2013) Feasibility study of using fine recycled concrete aggregate in producing self-consolidation concrete. J Sustain Cem-Based Mater 2(1):20–34
29. ASTM C 1761/1761 M - 17 (2017) Standard Specification for Lightweight Aggregate for Internal Curing of Concrete. American Society for Testing and Materials, USA
30. Kim JH, Choi SW, Lee KM, Choi YC (2018) Influence of internal curing on the pore size distribution of high strength concrete. Constr Build Mater 192:50–57
31. Ghourchian S, Wyrzykowski M, Lura P, Shekarchi M, Ahmadi B (2013) An investigation on the use of zeolite aggregates for internal curing of concrete. Constr Build Mater 40:135–144
32. Jensen OM, Lura P (2006) Techniques and materials for internal water curing of concrete. Mater Struct 39(9):817–825
33. Ge Z, Feng Y, Zhang H, Xiao J, Sun R, Liu X (2020) Use of recycled fine clay brick aggregate as internal curing agent for low water to cement ratio mortar. Constr Build Mater. https://doi.org/10.1016/j.conbuildmat.2020.120280
34. Efnarc S (2002) Guidelines for self-compacting concrete. London, UK: Association House 32:34
35. BSI, BS EN 206–9: (2010) Concrete. Additional rules for self-compacting concrete (SCC), BSI London, UK
36. NEN-EN 196–1 (2005) Methods of Testing Cement — Part 1: Determination of Strength. European Committee for Standardization
37. Zhang J, Scherer GW (2011) Comparison of methods for arresting hydration of cement. Cem Concr Res 41(10):1024–1036
38. Scrivener K, Snellings R, Lothenbach B (2018) A practical guide to microstructural analysis of cementitious materials, Crc Press
39. EW W (1921) Proceedings of the national academy of sciences, PNASA 7–21
40. Pfeifenberger MJ, Mangang M, Wurster S, Reiser J, Hohenwarter A, Pfleging W, Kiener D, Pippan R (2017) The use of femtosecond laser ablation as a novel tool for rapid micro-mechanical sample preparation. Mater Des 121:109–118
41. José Oliveira M, Ribeiro AB, Branco FG (2014) Combined effect of expansive and shrinkage reducing admixtures to control autogenous shrinkage in self-compacting concrete. Constr Build Mater. https://doi.org/10.1016/j.conbuildmat.2013.11.033
42. JGJ/T283-2012 (2012) Technical specification for application of self-compacting concrete. Ministry of Housing and Urban-Rural Development of the People's Republic of China
43. Carro-López D, González-Fonteboa B, de Brito J, Martínez-Abella F, González-Taboada I, Silva P (2015) Study of the

rheology of self-compacting concrete with fine recycled concrete aggregates. Constr Build Mater 96:491–501
44. Kou SC, Poon CS (2009) Properties of self-compacting concrete prepared with coarse and fine recycled concrete aggregates. Cem Concr Compos 31(9):622–627
45. Ye G (2003) Experimental study and numerical simulation of the development of the microstructure and permeability of cementitious materials. Cem Concr Res. https://doi.org/10.1016/S0008-8846(02)00891-8
46. Loukili A, Khelidj A, Richard P (1999) Hydration kinetics, change of relative humidity, and autogenous shrinkage of ultra-high-strength concrete. Cem Concr Res 29(4):577–584
47. Mendes A, Sanjayan JG, Gates WP, Collins F (2012) The influence of water absorption and porosity on the deterioration of cement paste and concrete exposed to elevated temperatures, as in a fire event. Cem Concr Compos 34(9):1067–1074
48. Knapen E, Cizer Ö, Van Balen K, Van Gemert D (2006) Comparison of solvent exchange and vacuum drying techniques to remove free water from early age cement-based materials. Proceedings of 2nd International RILEM Symposium on Advances in Concrete through Science and Engineering, Quebec, Canada, September 11–13, Rilem Publications SARL, France
49. Odler I, Abdul-Maula S (1984) Possibilities of quantitative determination of the AFt-(ettringite) and AFm-(monosulphate) phases in hydrated cement pastes. Cem Concr Res 14(1):133–141
50. De Weerdt K, Haha MB, Le Saout G, Kjellsen KO, Justnes H, Lothenbach B (2011) Hydration mechanisms of ternary Portland cements containing limestone powder and fly ash. Cem Concr Res 41(3):279–291
51. Wang A, Zhang C, Sun W (2004) Fly ash effects: II: the active effect of fly ash. Cem Concr Res 34(11):2057–2060
52. Scrivener KL, Pratt PL (1996) Characterization of interfacial microstructure. Interfacial transit zone concr 2:3–18
53. Lo T, Cui H (2004) Effect of porous lightweight aggregate on strength of concrete. MatL 58(6):916–919
54. Zaitsev Y, Wittmann F (1981) Simulation of crack propagation and failure of concrete. Materiaux et Construction 14(5):357–365
55. Van Mier JG (2012) Concrete fracture: a multiscale approach, CRC press
56. Zhang H, Šavija B, Chaves Figueiredo S, Lukovic M, Schlangen E (2016) Microscale Testing and modelling of cement paste as basis for multi-scale modelling. Materials. https://doi.org/10.3390/ma9110907
57. Zhang H, Xu Y, Gan Y, Chang Z, Schlangen E, Šavija B (2019) Combined experimental and numerical study of uniaxial compression failure of hardened cement paste at micrometre length scale, Cem Concr Res 126:105925
58. Zhang H (2019) Experimentally validated multi-scale fracture modelling scheme of cementitious materials, Delft University of Technology
59. Gesoglu M, Güneyisi E, Öz HÖ, Taha I, Yasemin MT (2015) Failure characteristics of self-compacting concretes made with recycled aggregates. Constr Build Mater 98:334–344
60. Grdic ZJ, Toplicic-Curcic GA, Despotovic IM, Ristic NS (2010) Properties of self-compacting concrete prepared with coarse recycled concrete aggregate. Constr Build Mater 24(7):1129–1133
61. Bordelon A, Cervantes V, Roesler JR (2009) Fracture properties of concrete containing recycled concrete aggregates. Mag Concr Res 61(9):665–670
62. Alengaram UJ, Salam A, Jumaat MZ, Jaafar FF, Saad HB (2011) Properties of high-workability concrete with recycled concrete aggregate. Mater Res 14(2):248–255
63. Mehta PK, Monteiro PJ (2017) Concrete microstructure, properties and materials. McGraw-Hill Education
64. Wei Y, Hansen W, Biernacki JJ, Schlangen E (2011) Unified shrinkage model for concrete from autogenous shrinkage test on paste with and without ground-granulated blast-furnace slag. ACI Mater J 108(1):13
65. Jonasson J, Groth P, Hedlund H (1994) Modelling of temperature and moisture field in concrete to study early age movements as a basis for stress analysis, Thermal Cracking in Concrete at Early Ages: Proceedings of the International RILEM Symposium, CRC Press 45–54
66. Wei Y, Xiang Y, Zhang Q (2013) Internal curing efficiency of prewetted LWFAs on concrete humidity and autogenous shrinkage development. J Mater Civ Eng 26(5):947–954
67. Pickett G (1956) Effect of aggregate on shrinkage of concrete and a hypothesis concerning shrinkage. J Proc 52(1):581–590
68. Tianshi L (2019) Autogenous shrinkage of early age cement paste and mortar. Delft University of Technology, Delft, The Netherlands